Heliyon 9 (2023) e20750

Contents lists available at ScienceDirect

Heliyon

journal homepage: www.cell.com/heliyon

Screening for osteoporosis based on IQon spectral CT virtual low monoenergetic images: Comparison with conventional 120 kVp images☆

Hehui Zhang [a,1], Wen Wei [a,1], Baoxin Qian [b], Daoqin Wu [a], Cunhong Zheng [a], Honghua Li [a], Jinsong Tang [a,*]

[a] The Second Affiliated Hospital of Fujian University of Traditional Chinese Medicine, Fuzhou, Fujian, China
[b] Huiying Medical Technology Co., Ltd, Beijing City, 100192, China

ARTICLE INFO

Keywords:
Spectral CT
Virtual monoenergetic images
Osteoporosis screening
Machine learning

ABSTRACT

Objectives: To explore the differences between low kiloelectron volt (keV) virtual monoenergetic images (VMIs) using IQon spectral CT and conventional CT (120 kVp) in the diagnosis of osteoporosis.

Methods: This retrospective study included 317 patients who underwent IQon spectral CT and dual-energy X-ray absorptiometry (DXA) examination. Commercial deep learning–based software was used for the fully automated extraction of the CT values of the first to fourth lumbar vertebrae (L1–L4) from two different low-keV levels (including 40/70 keV) VMIs and conventional 120 kVp images. The DXA examination results served as the standard of reference (normal [T-score ≥ -1], osteopenia [$-2.5 <$ T-score < -1], and osteoporosis [T-score < -2.5]). Osteoporosis diagnosis models were constructed using machine learning classifiers (logistic regression, support vector machine, random forest, XGBoost, and multilayer perceptron) based on the average CT values of L1–L4. The area under the receiver operating characteristic curve (AUC) and DeLong test were performed to compare differences in the performance of the osteoporosis diagnosis model between virtual low-keV VMIs and standard 120 kVp images.

Results: Random forest-based prediction model obtained good overall performance among all classifiers, and macro/micro average AUC values of 0.820/840, 0.834/853, and 0.831/852 were obtained based on 40/70 keV and 120 kVp images, respectively. The model presented no significant difference between low-keV VMIs and standard 120 kVp images for the diagnosis of osteoporosis ($p > 0.05$).

Conclusions: The performance of the osteoporosis diagnosis model using IQon spectral CT simulating the low tube voltage scanning condition (less than 120 kVp) was also satisfactory. Bone density screening evaluation can be performed with a combination of low-dose lung scanning CT, greatly reducing the radiation dose without affecting the diagnosis.

☆ This work was funded by the Grant of Science and Technology Commission of Fujian Province (Grant number: 2020Y0043).

* Corresponding author. The Second Affiliated Hospital of Fujian University of Traditional Chinese Medicine Fuzhou, Fujian, 350001, China.
E-mail address: tang-98@126.com (J. Tang).
[1] Co-First authors: Hehui Zhang and Wen Wei. The first two authors contributed equally to this study.

https://doi.org/10.1016/j.heliyon.2023.e20750
Received 6 July 2023; Received in revised form 24 September 2023; Accepted 5 October 2023
Available online 12 October 2023

1. Introduction

Osteoporosis is a systemic disease characterised by decreased bone mass and density, resulting in increased bone fragility and susceptibility to fracture [1,2]. Although there are no obvious symptoms in the early stages of osteoporosis, it is harmful when osteoporosis progresses to later stages. In China, people over 60 years old account for 36 % of osteoporosis patients, and the total number of patients exceeds 90 million [3,4]. With the aging population becoming increasingly prevalent, osteoporosis is clinically called the "silent killer" of the elderly [5] and seriously endangers patients' health. Currently, the diagnosis and treatment of osteoporosis in China are not ideal. Osteoporosis fracture is one of the main causes of disability and death in elderly patients and is most commonly seen in vertebral and femoral head fractures [6]. Moreover, the quality of life of the elderly is greatly affected after a fracture and leads to irreversible disability, causing a heavy medical burden on families and society. However, osteoporosis can be prevented and treated; therefore, timely screening of abnormal bones is significant for subsequent protection and treatment [7].

Bone mineral density (BMD) measurements such as dual-energy X-ray absorptiometry (DXA) and quantitative computed tomography (QCT) are the main bases for diagnosis. QCT uses clinical CT scan data; therefore, QCT and CT are closely related in nature, and ionising radiation is receiving increasing attention with the widespread use of CT. Under the premise of achieving the best balance between radiation dose and image quality, the general trend for low-dose computed tomography (LDCT) inspection is to effectively reduce the CT radiation dose by reducing the tube voltage as much as possible, reducing the tube current, and increasing the pitch [8]. Therefore, in clinical practice, reducing the dose of CT scans to make the examination safer is an important issue of clinical research. Specifically, the IQon spectral CT is equipped with a unique two-layer detector structure to receive high- and low-energy X-ray photons, respectively, to distinguish between high- and low-energy mixed-level X-rays, and can obtain spectral images and conventional images simultaneously. Spectral images usually include: virtual monoenergetic images (VMIs), virtual scan (VNC), iodine density (Z Effective) images, and other 12 categories, which can be used in a variety of different clinical applications and research; furthermore, monoenergetic image is equivalent to single-energy X-ray imaging (including 40–200 keV, 161 single-energy) and is very conducive to the study of low dose synchronization between QCT and clinical CT scan.

Artificial intelligence (AI) 's rapid development has made it widely used in various fields. Although its application in the treatment of osteoporosis has just begun, it shows good prospects [9]. Specifically, Fang et al. [10] developed a fully automatic method based on a deep convolutional neural network (DCNN) for vertebral body segmentation and bone BMD calculation in CT images; the average BMDs calculated showed high correlation ($r > 0.98$) and agreement with those derived from QCT. Yasaka et al. [11] used DXA as the gold standard to predict lumbar BMD in unenhanced abdominal CT images based on the deep learning method, and the final effective AUC reached 0.965, indicating that the AI method can be used to predict BMDs in CT images. Furthermore, Yao et al. [12]developed a radiomics nomogram incorporating radiomics features and clinical factors based on fat-water imaging of dual-energy spectral CT, which may serve as an efficient tool for distinguishing abnormally low BMD from normal BMD.

In this study, using a combination of machine learning technology and CT image features, we used machine learning to develop an osteoporosis diagnosis model and explored whether there was a statistically significant difference in the performance of the model between the vertebral CT value of low-keV VMIs and that of standard 120 kVp images.

2. Materials and methods

The relevant institutional review board approved this retrospective study and waived the requirement for study-specific informed consent.

2.1. Patients and data collection

We retrospectively analysed patients treated at our institution between January 2021 and December 2022. The inclusion criteria were as follows: (1) the same sample was scanned by lumbar CT and lumbar DXA with IQon Spectral CT and Hologic Discovery, and the interval between the two examinations was less than 24 h; (2) the sample data selected should include CT images of the L1–L4 vertebrae in the lumbar spine, and each sample data should contain 40/70 keV and 120 kVp images. The exclusion criteria were incomplete image data and artefacts in the image that could not be marked or excluded. A total of 320 cases were collected during this period, including three cases whose data were incomplete and excluded. Finally, 317 patients were included in this study (166 males and 151 females), whose ages ranged from 27 to 83 years, with an average age of 51.26 years old.

2.2. IQon spectral CT

In the real world, lumbar CT examinations of the same subject cannot be performed in the same time period under different scanning conditions, and conventional equipment cannot guarantee the unity of simultaneous homology of images. Therefore, we used IQon spectral CT to obtain the virtual monoenergetic 40/70 keV parameters simultaneously. For the SBI parameters of spectral CT, monoenergetic 40/70 KeV images were selected to simulate scanning conditions of less than 120 kVp. Notably, kVp is the maximum voltage applied to the entire X-ray tube, which is called 120 kV (120 kVp) in traditional CT. Moreover, keV (virtual monoenergetic image) can reduce the negative image effects of mixed energy, such as reducing noise and hardening beam artefacts, and enhancing tissue contrast.

Research shows that when kVp decreases, the CT value increases, which increases the contrast of the image; however, the radiation dose can be significantly decreased [13,14]. The CT value of the 65–75 keV single-energy image was almost the same as that of the

traditional image generated at conventional 120 kVp, see Figure (1A-1B), while the CT value of the low-kVp scan image was larger than that of the 120 kVp image (Fig. 1C). Therefore, monoenergetic 40/70 keV single-energy images can be simulated to be equivalent to images generated at voltages less than the conventional 120 kVp.

The equipment was characterised using IQon Spectral CT. The imaging parameters were as follows: voltage, 120 kVp; current, 182 mA; thickness, 1 mm; interval increment, 1 mm; pitch, 0.984; rotation time = 0.75 s/turn. scan time = 7.1 s, recon mode iDose4 level = 3, filter standard = B, field of view = 250 mm, rebuild matrix = 512 × 512.

2.3. DXA examinations

All patients underwent routine DXA using a scanner (Hologic Discovery, APEX Process 3.3.01). The parameters were as follows: voltage, 140/100 kVp; current, = 2.5 mA, frequency 50 Hz; line spacing, 0.1008 cm; point resolution, 0.0901 cm; and lumbar spine scanning sites.

2.4. Diagnostic criteria for osteoporosis

DXA of the lumbar spine was performed for BMD assessment using standard techniques according to the manufacturer's and WHO guidelines (Hologic Discovery dual-energy X-ray bone densitometer; Hologic Inc., Bedford, MA) [15]. According to the WHO guidelines, a DXA-derived T-score less than −1.0 indicates an abnormally low BMD, which is further categorised into osteopenia (T-score between −1.0 and−2.5) and osteoporosis (T-score of −2.5 or below), and a T-score greater than −1.0 is normal. In our study, the patients were divided into three groups according to T-score: normal BMD (T-score ≥ −1), osteopenia (−2.5 < T-score < −1), and osteoporosis (T-score < −2.5).

2.5. CT value measurement based on automatic AI solution

A deep learning-based, commercially available, automatic AI solution (Quantitative CT-Assisted Diagnosis Dystem, Huiying Medicine Technology, China, hereafter referred to as software) was used for fully automatic vertebral segmentation and CT value extraction. A detailed visualisation of automatic AI solutions is shown in Fig. 2A. As illustrated in Fig. 2A, the Automatic AI solution contained two parts: vertebral segmentation and CT value extraction (Hounsfield units, HU). Firstly, 40/70 keV VMIs and conventional

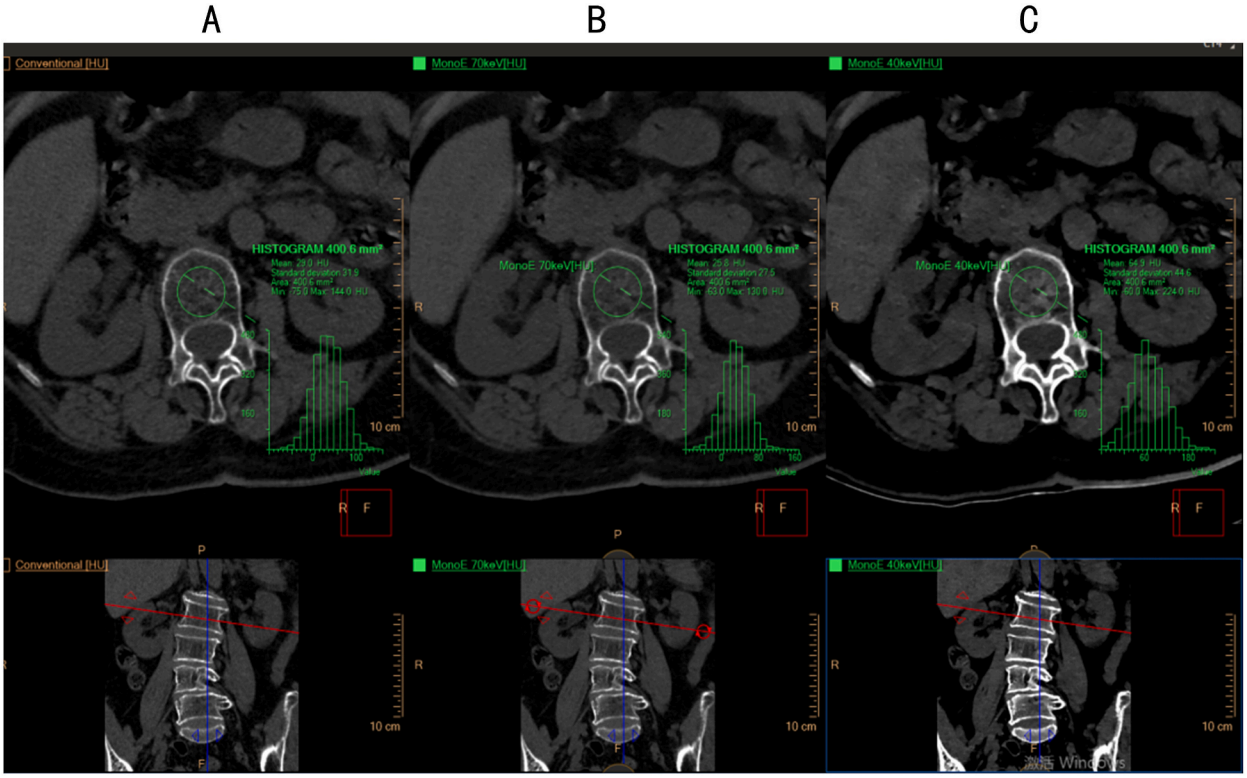

Fig. 1. Virtual low energy IQon CT image. The CT values of the same vertebral body in the same patient under different (A) 120 kVp, (B) 70 keV and (C) 40 keV conditions. CT (120 kV) = 30Hu, CT (70 keV) = 26Hu, CT (40 keV) = 54.4Hu; CT (120 kV) and CT (70 keV) values are almost the same; CT (40 keV) > CT (120 kV).

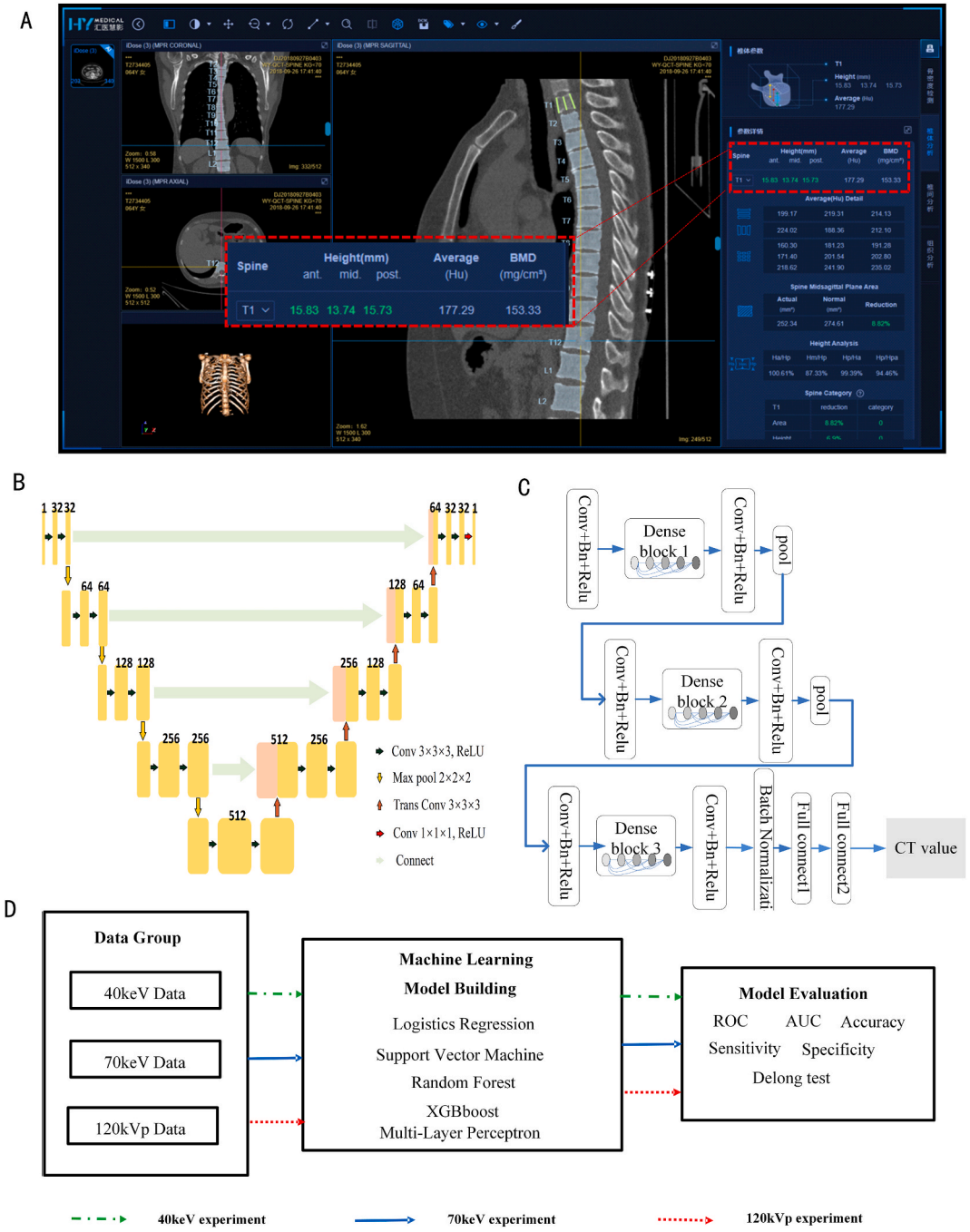

Fig. 2. Method flow chart. (A) Automatic AI solution, (B) U-net network for vertebra segmentation, (C) DenseNet network for CT value extraction, (D) machine learning model building for osteoporosis screening.

120 kVp images containing the lumbar vertebrae were inputted into the software. Based on the deep learning segmentation algorithm, the software could then accurately locate and segment the first lumbar vertebra into the fourth lumbar vertebra (L1–L4). The U-Net network was used in the AI software. Specifically, the U-Net network has a U-shaped network structure (see Fig. 2B) consisting of the left and right halves of the coding and decoding networks, respectively. Furthermore, feature fusion between the coding and decoding modules was performed using a skip connection to obtain the location information. Fig. 3 **A1-C2** shows the vertebral body obtained by the U-Net segmentation model of different keV images of the same patient using this software. The software had stable performance and did not cause a significant difference in segmentation with the change in voltage level.

After segmentation of the vertebral bodies, the CT values of the vertebral bodies were directly extracted in batches using software.

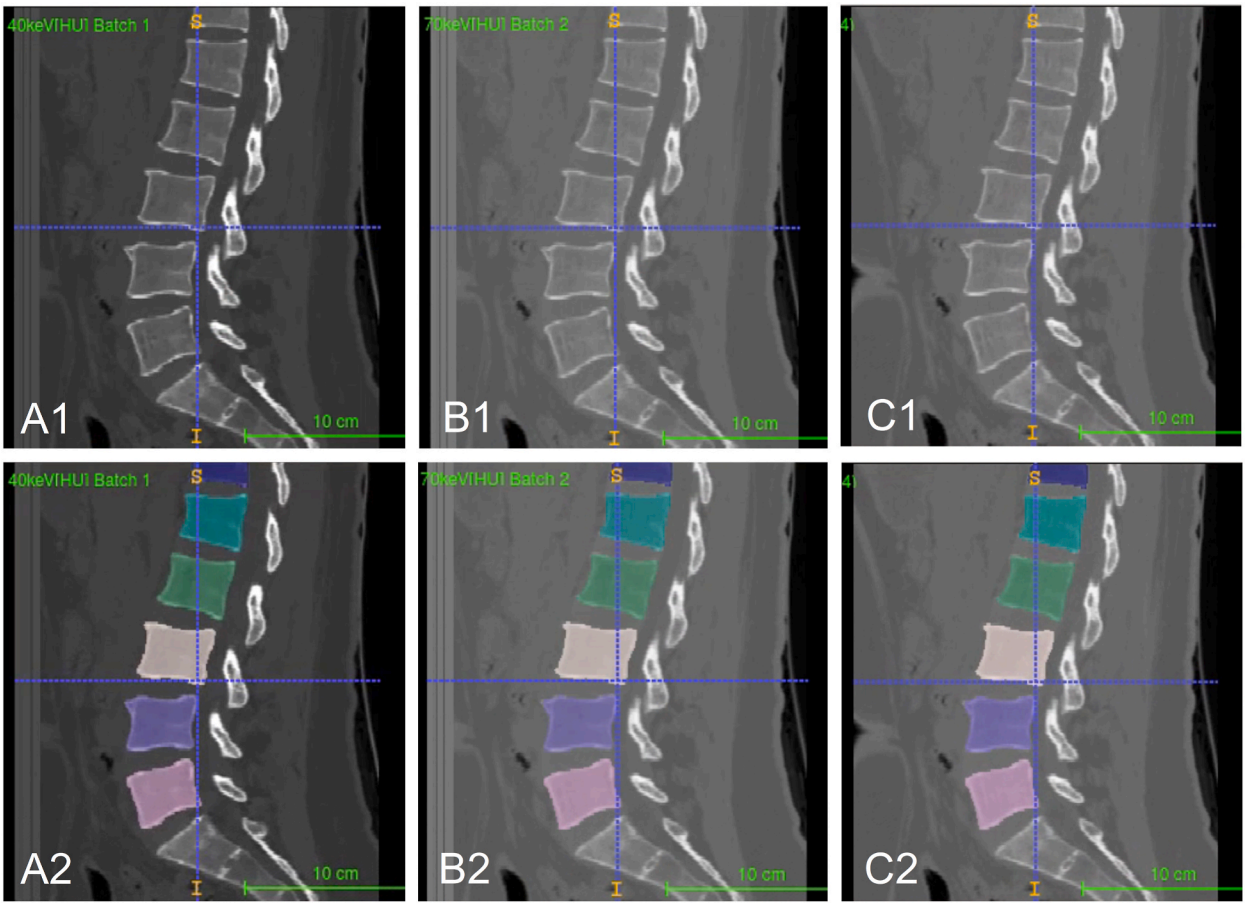

Fig. 3. Results of AI automatic segmentation of lumbar vertebrae for 40 keV (A1, A2), 70 keV (B1, B2) and 120 kVp (C1, C2). (A1, B1, C1) The original image. (A2, B2, C2) AI segmentation results.

Table 1
Demographic characteristics of all patients in the training and test sets.

	Level	Overall	Training set	Test set	p
		(N = 317)	(N = 220)	(N = 97)	
age (mean (SD))		51.48 (11.34)	51.61 (11.51)	51.20 (11.01)	0.7655
sex (%)					1.0000
	Male	153 (48.26)	106 (48.18)	47 (48.45)	
	Female	164 (51.74)	114 (51.82)	50 (51.55)	
label (%)					0.9862
	Normal	164 (51.74)	114 (51.82)	50 (51.55)	
	Osteopenia	112 (35.33)	78 (35.45)	34 (35.05)	
	Osteoporosis	41 (12.93)	28 (12.73)	13 (13.40)	
L1_CTvalue_120 kVp(mean (SD))		187.57 (58.29)	186.34 (57.96)	190.37 (59.22)	0.5716
L2_CTvalue_120 kVp(mean (SD))		177.98 (58.79)	176.21 (56.48)	182.01 (63.86)	0.4191
L3_CTvalue_120 kVp(mean (SD))		165.51 (57.35)	165.90 (56.36)	164.61 (59.81)	0.8530
L4_CTvalue_120 kVp(mean (SD))		169.59 (59.88)	170.22 (59.07)	168.16 (61.95)	0.7780
L1_CTvalue_40 keV (mean (SD))		425.18 (129.56)	425.09 (130.72)	425.39 (127.56)	0.9848
L2_CTvalue_40 keV (mean (SD))		412.56 (129.95)	409.72 (127.83)	419.01 (135.07)	0.5583
L3_CTvalue_40 keV (mean (SD))		396.73 (129.47)	396.31 (130.35)	397.70 (128.11)	0.9297
L4_CTvalue_40 keV (mean (SD))		407.85 (135.47)	406.63 (136.46)	410.62 (133.87)	0.8096
L1_CTvalue_70 keV (mean (SD))		194.38 (60.02)	193.50 (60.19)	196.36 (59.91)	0.6965
L2_CTvalue_70 keV (mean (SD))		186.82 (61.05)	185.14 (59.77)	190.63 (64.01)	0.4617
L3_CTvalue_70 keV (mean (SD))		176.75 (61.45)	176.28 (61.58)	177.84 (61.47)	0.8351
L4_CTvalue_70 keV (mean (SD))		182.01 (64.13)	181.56 (64.30)	183.04 (64.05)	0.8505

The regression algorithm adopted by the AI system in this study was the deep learning Densenet121 model. First, a CNN structure is used as the backbone to extract image features, and the basic units in DenseNet are dense blocks (DB). The DB module comprises convolution layers (Conv), batch normalisation layers (BN), and ReLU activation function layers (Conv-BN-ReLU). The connect (FC) part was added as the regression detection head to the output results, and the output value was the CT value predicted by the model. Fig. 2C shows a schematic of image prediction using DenseNet. Furthermore, all patient images were input into the AI system, and CT values of the L1-L4 vertebra of each patient were obtained in batches, which were recorded to construct the machine learning model for osteoporosis screening. According to the images at different keV (40/70 keV and 120 kVp), the CT values of L1, L2, L3, and L4 for each patient were extracted, with a total of 12 values.

2.6. Machine learning model construction for osteoporosis screening

This study did the following work for the triple classification (normal BMD, osteopenia, and osteoporosis). The construction of the machine learning model is illustrated in Fig. 2D. The average CT values of L1–L4 from 40/70 keV VIMs and those of L1–L4 from conventional 120 kVp images were used for model construction; therefore, we performed three group experiments: Experiment 1 (based on 40 keV data), Experiment 2 (based on 70 keV data), and Experiment 3 (based on 120 kVp data). In the different experiments, 70 % of the data were used to develop a predictive model, and the remaining data were used to evaluate the model's performance.

Before data analysis, all missing values were replaced with the median of the current category. Moreover, data was standardised using the z-score method. The dataset was randomly divided into training and test sets at a ratio of 7:3 while ensuring the same distribution of categories in the grouping. Five distinct machine learning classifiers were employed to develop an osteoporosis diagnosis model. These classifiers encompass Logistic Regression (LR), Support Vector Machine (SVM), Random Forest (RF), XGBoost, and a Multilayer Perceptron (MLP). The hyperparameters of each classifier were meticulously tuned using gridSearch, with their respective configurations detailed in Table 2.

The two most popular strategies for multiclass machine learning are the "one against one" [16], which builds one classifier for each pair of classes, and the "one against rest" [17], which consists of building one classifier per class and is trained to distinguish the samples in a single class from the samples in all remaining classes. In this study, we chose "one against rest" for classification.

2.7. Statistical analysis

The Shapiro-Wilk test was used to test the normality of all continuous variables. The *t*-test or Wilcoxon rank-sum test was used to compare normally or abnormally distributed continuous variables between the groups. Chi-squared or Fisher's exact tests were used for qualitative data analysis. The characteristics were examined using R 4.2.1. A two-sided $P < 0.05$ was considered statistically significant. The remaining data were analysed using Scikit-learn based on Python 3.9. The performances of the models were estimated using receiver operating characteristic (ROC) curves, the area under the curve (AUC), overall accuracy (OA), sensitivity, and specificity. DeLong tests were performed to compare the significant differences in performance between different machine learning classifiers and those of different experiments.

3. Result

3.1. Patients characteristics

Table 1 summarises the demographic characteristics of patients. A total of 317 patients were divided into training (n = 220) and test sets (n = 97) in a ratio of 7:3. The average age for all patients was 51.48 ± 11.34 years, with 153 males and 164 females. The patients were classified into three groups according to DXA guidelines: normal (n = 164), osteopenia (n = 112), and osteoporosis (n = 41). There were no statistically significant differences in demographic characteristics between the training and test sets (all $p > 0.05$).

3.2. Diagnostic performance

Table 3 displays the macro/micro average AUC (Ma-auc and Mi-auc), accuracy (Acc), sensitivity (Sen), and specificity (Spec) for various classifiers across distinct experiments. Notably, the RF model exhibited robust macro-/micro-average AUC in the training cohort, and this consistent performance carried over to the test sets in Experiment 1, Experiment 2, and Experiment 3. Across these experiments, the RF-based three-class prediction model consistently showcased strong overall performance, yielding Ma-aucs/Mi-auc

Table 2
The classifier's hyperparameter settings.

Classifier	Settings
LR	penalty = 'l2',class_weight = 'unbalanced', C = 1
SVM	C = 10, kernel = 'linear', probability = True, class_weight = 'unbalanced'
RF	n_estimators = 60, max_depth = 2, max_features = 'auto', random_state = 101
XGBoost	max_depth = 3, learning_rate = 0.1, n_estimators = 10
MLP	solver = 'adam', alpha = 1e-4, hidden_layer_sizes=(5, 2), random_state = 101

Table 3
Performance comparison of different machine learning classifiers based on different experiments.

Experiment	Classifier	Training set					Test set				
		Ma-auc	Mi-auc	Acc	Sen	Spec	Ma-auc	Mi-auc	Acc	Sen	Spec
40 keV	LR	0.782	0.797	0.595	0.595	0.798	0.811	0.822	0.619	0.619	0.809
	SVM	0.806	0.834	0.605	0.605	0.802	0.820	0.839	0.608	0.608	0.804
	RF	0.836	0.861	0.677	0.677	0.839	0.820	0.840	0.670	0.670	0.835
	XGBoost	0.871	0.887	0.736	0.736	0.868	0.810	0.834	0.629	0.629	0.814
	MLP	0.832	0.857	0.650	0.650	0.825	0.815	0.840	0.660	0.660	0.830
70 keV	LR	0.791	0.804	0.609	0.609	0.805	0.816	0.827	0.619	0.619	0.809
	SVM	0.807	0.835	0.605	0.605	0.802	0.822	0.838	0.680	0.680	0.840
	RF	0.922	0.928	0.795	0.795	0.898	0.834	0.853	0.680	0.680	0.840
	XGBoost	0.870	0.890	0.727	0.727	0.864	0.818	0.842	0.660	0.660	0.830
	MLP	0.824	0.851	0.668	0.668	0.834	0.828	0.843	0.660	0.660	0.830
120 kVp	LR	0.819	0.839	0.682	0.682	0.841	0.809	0.828	0.649	0.649	0.825
	SVM	0.827	0.850	0.623	0.623	0.811	0.808	0.833	0.619	0.619	0.809
	RF	0.886	0.897	0.736	0.736	0.868	0.831	0.852	0.660	0.660	0.830
	XGBoost	0.894	0.905	0.723	0.723	0.861	0.817	0.846	0.660	0.660	0.830
	MLP	0.829	0.856	0.677	0.677	0.839	0.821	0.846	0.680	0.680	0.840

values of 0.820/840, 0.834/853, and 0.831/852, respectively, based on 40 keV, 70 keV, and 120 kVp images. It is important to highlight that there were no statistically significant differences in classifier performance across different categories ($p > 0.05$), as outlined in Table 4.

Fig. 4 A-F presents the three-class (one-vs.-rest) ROC curves for the random forest model in various experiments. In the test sets of experiments 1, 2, and 3, the discrimination AUC values were 0.846/851/0.864 for the normal group, 0.740/770/710 for osteopenia, and 0.853/0.867/0.895 for the osteoporosis group, respectively. The RF model consistently demonstrated its efficacy in distinguishing normal from abnormal bone mineral density (BMD) and identifying osteoporosis cases.

Additionally, Fig. 5 A-B comprehensively compares the RF model's performance across different experiments. It is evident that the RF model excelled in specificity compared to its overall accuracy. The DeLong test results between low-energy images and 120 kVp images, as detailed in Table 5, revealed that spectral CT images at simulated low tube voltage conditions (40 keV and 70 keV) did not exhibit significant differences in qualitative osteoporosis analysis when compared to standard 120 kVp images ($p > 0.05$).

4. Discussion

At present, in the risk prediction and curative effect evaluation of osteoporosis, some studies have shown similar diagnostic accuracy of QCT and DXA for diagnosing osteoporosis [18]. In this study, we used DXA examination results as the reference standard and trained and tested a machine-learning model that could differentiate changes in the average CT values of the L1–L4 vertebrae. More importantly, Li et al. found that osteoporosis screening could be accurately performed using either QCT or spectral CT, which had a smaller bias than QCT [19]. Current diagnostic criteria for DXA are based on 120 kVp measurement results, and a low-dose technique is recommended [20]. In this study, we used spectral CT to simulate a low-dose voltage situation, and multiple sets of images of different conditions were acquired simultaneously. Furthermore, we chose 40/70 keV and 120 kVp images to extract the CT values of the L1–L4 vertebrae.

To the best of our knowledge, this is one of the few studies investigating the effect of different tube voltages on the performance of osteoporosis models based on spectral CT. We trained multiple machine learning models for triple classification tasks based on CT values using 40/70 keV and 120 kVp data and assessed whether the results were statistically significantly different. We found that different machine learning models performed better on both the training and test sets, with the model constructed using the random forest method performing the best. In terms of comparing model significance using the Delong test, there were no statistically significant differences in model performance between the categories ($p > 0.05$), except for the individual methods. The spectral image data from the two simulated low tube voltage conditions, 40kev or 70kev, presented no significant difference in the qualitative analysis

Table 4
DeLong test results between RF and other machine learning classifiers based on test set.

Experiment	Class	LR	SVM	XGBoost	MLP
40 keV	Normal	0.938	0.525	0.612	0.837
	Osteopenia	0.530	0.762	0.425	0.855
	Osteoporosis	0.569	0.423	0.211	0.502
70 keV	Normal	0.930	0.780	0.885	0.694
	Osteopenia	0.302	0.428	0.414	0.631
	Osteoporosis	0.263	0.465	0.312	0.398
120 kVp	Normal	0.433	0.117	0.353	0.255
	Osteopenia	0.422	0.818	0.754	0.533
	Osteoporosis	0.367	0.261	0.530	0.608

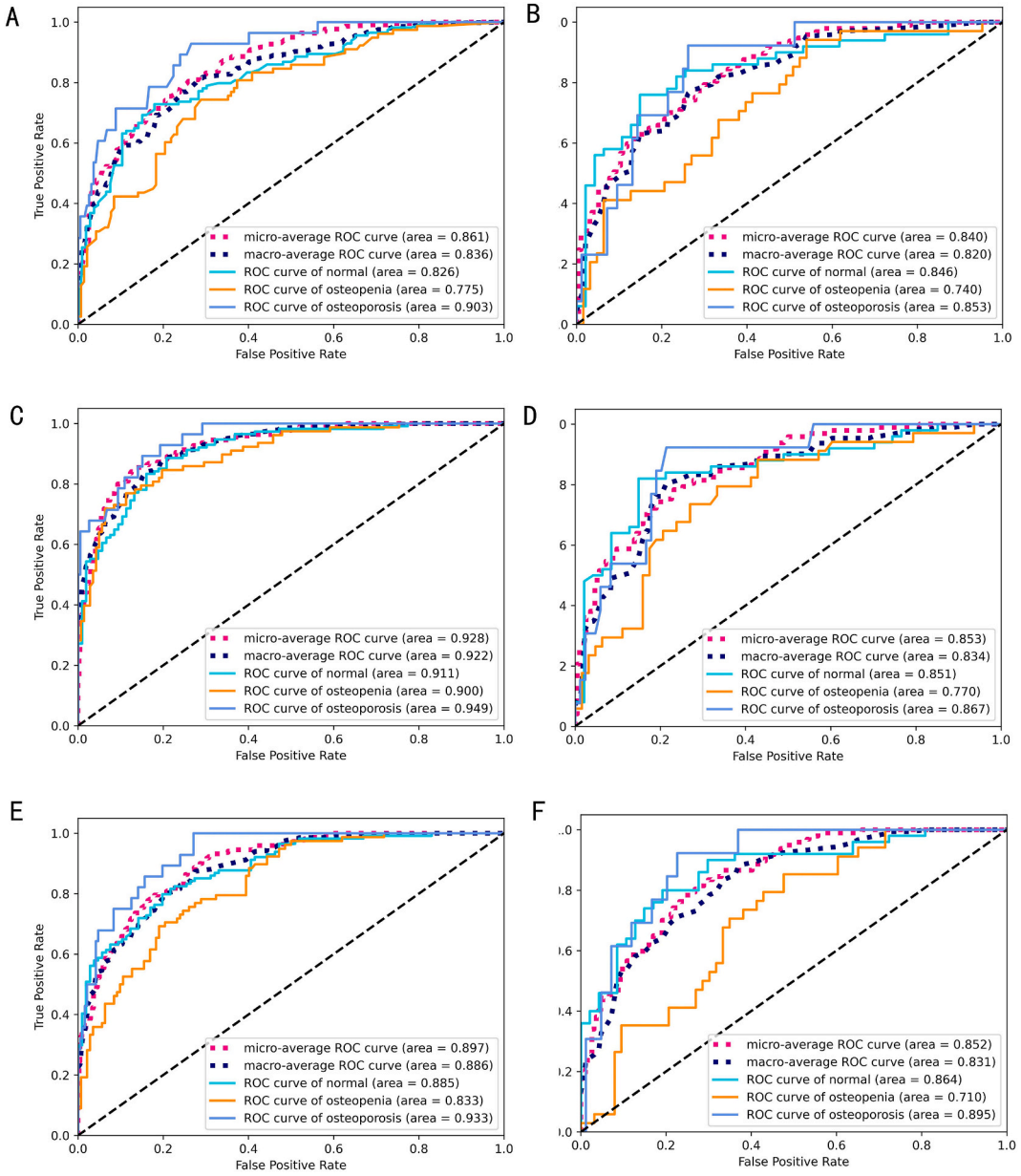

Fig. 4. Three-class (one-vs-rest) ROC curves of random forest model for different experiments. Result base on based on 40 keV data in training (A) and test (B) sets; result base on based on 70 keV data in training (C) and test (D) sets; result base on based on 120 kVp data in training (E) and test (F) sets. The two dashed lines respectively show the ROC curves of micro-average and macro-average, indicating the overall distinguishing ability of the three-class classification.

of osteoporosis when compared with the standard 120 kVp images. Spectral-detector CT virtual low-energy imaging has very high sensitivity and specificity for osteoporosis monitoring [21].

Several limitations are associated with this study. Firstly, the extraction of CT values relied on vertebral body segmentation performed by artificial intelligence software. Notably, not all segmented vertebral body masks were manually corrected, possibly leading to biases in the CT values for certain patients. Secondly, the scope of the dataset was limited, and a multi-centre experiment was not conducted. This restricted the data's diversity and the findings' potential applicability to broader populations. Lastly, the study did not encompass the validation of the model's generalizability under higher tube voltages. Future investigations are planned to address these limitations and provide insights into the model's performance across these dimensions.

In conclusion, the performance of the osteoporosis diagnosis model using IQon spectral CT simulating the low tube voltage scanning condition (less than 120 kVp) was also satisfactory. Bone density screening evaluation can be performed with a combination of LDCT data without increasing the radiation dose and scanning time so that the subject receives one radiation examination and

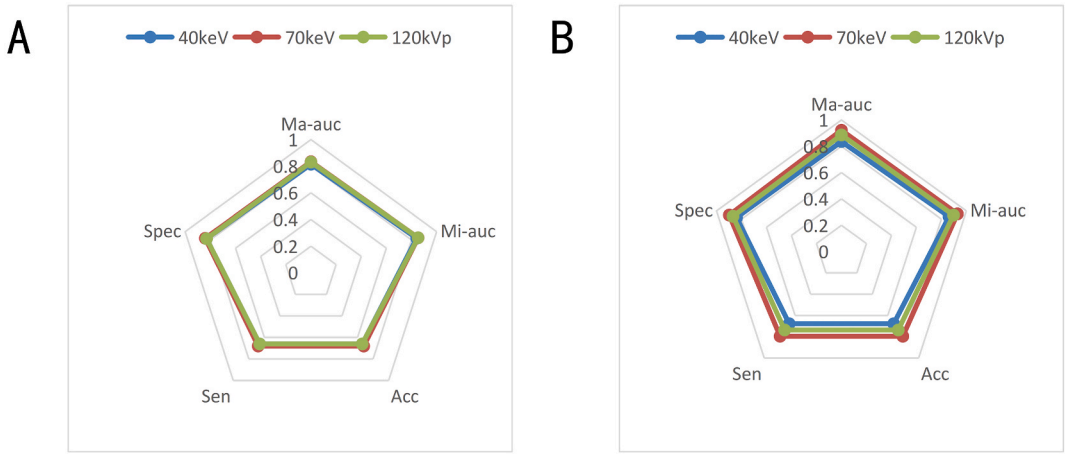

Fig. 5. Compare the model performance of different experiments with multiple indexes. (A) Training set and (B) test set.

Table 5
DeLong test results between low energy images and 120 kVp based on test set.

	Experiment (AUC)			Delong Test (*P*-value)	
	40 keV	70 keV	120 kVp	40 keV vs 120 kVp	70 keV vs 120 kVp
Normal	0.846	0.851	0.864	0.856	0.642
Osteopenia	0.740	0.770	0.710	0.713	0.810
Osteoporosis	0.853	0.867	0.895	0.298	0.565

obtains multiple results to achieve multi-disease co-examination. This model has wide application prospects in physical examinations [22].

Funding

This work was funded by the Grant of Science and Technology Commission of Fujian Province (Grant number: 2020Y0043). The funders played no role in the study design, data collection or analysis, the decision to publish, or manuscript preparation.

Data availability statement

The data of this study are available on request from the corresponding author. The data are not publicly available due to privacy or ethical restrictions.

CRediT authorship contribution statement

Hehui Zhang: Conceptualization, Data curation, Visualization, Writing – original draft, Writing – review & editing. **Wen Wei:** Conceptualization, Data curation, Formal analysis, Visualization, Writing – original draft, Writing – review & editing. **Baoxin Qian:** Conceptualization, Data curation, Formal analysis, Investigation, Methodology, Software, Visualization, Writing – original draft, Writing – review & editing. **Daoqin Wu:** Data curation, Formal analysis, Funding acquisition, Investigation, Methodology, Validation. **Cunhong Zheng:** Data curation, Formal analysis, Funding acquisition, Methodology, Project administration, Resources. **Honghua Li:** Data curation, Formal analysis, Investigation, Methodology. **Jinsong Tang:** Conceptualization, Data curation, Formal analysis, Funding acquisition, Investigation, Methodology, Project administration, Resources, Supervision, Validation, Visualization, Writing – original draft, Writing – review & editing.

Declaration of competing interest

The authors declare that they have no known competing financial interests or personal relationships that could have appeared to influence the work reported in this paper.

References

[1] J.A. Kanis, L.J. Melton 3rd, C. Christiansen, et al., The diagnosis of osteoporosis, J. Bone Miner. Res. 9 (8) (1994) 1137–1141.

[2] L. Jia, The value of vertebral bone mineral density measurement with dual energy X-ray absorptiometry in 100 cases of osteoporosis, Imaging Res. Med. Appl. 2 (17) (2018) 122–123.
[3] X.G. Cheng, S.Y. Dong, L. Wang, et al., Prevalence of osteoporosis in China: a multicenter, large scale survey of a health checkup population, Chin. J. Health Manag. 13 (1) (2019) 51–58.
[4] Q. Zeng, N. Li, Q. Wang, et al., The prevalence of osteoporosis in China, a nationwide, multicenter DXA survey, J. Bone Miner. Res. 34 (10) (2019) 1789–1797.
[5] E.K. Osnes, C.M. Lofthus, H.E. Meyer, et al., Consequences of hip fracture on activities of daily life and residential needs, Osteoporos Int. 15 (2004) 567–574.
[6] E.S. Siris, R. Adler, J. Bilezikian, et al., The clinical diagnosis of osteoporosis:a position statement from the national bone health alliance working group, Osteoporos Int. 25 (5) (2014) 1439–1443.
[7] W.B. Xia, Z.H. Zhang, C. Wang, et al., Primary osteoporosis diagnosis and treatment guidelines (2017), Chin. J. Osteoporos. 25 (3) (2019) 281–309.
[8] Working group on guidelines for diagnosis and treatment of senile osteoporosis in China (2018), Osteoporosis Society of China Association of Gerontology and Geriatrics. 2018 China guideline for diagnosis and treatment of senile osteoporosis), Chin. J. Osteoporos. 24 (12) (2018) 1541–1567.
[9] T. Bartalena, M.F. Rinaldi, C. Modolon, et al., Incidental vertebral compression fractures in imaging studies: lessons not learned by radiologists, World J. Radiol. 2 (2010) 399–404.
[10] Y.J. Fang, et al., Opportunistic osteoporosis screening in multi-detector CT images using deep convolutional neural networks, Eur. Radiol. 31 (2021) 1831–1842.
[11] K. Yasaka, H. Akai, A. Kunimatsu, S. Kiryu, O. Abe, Prediction of bone mineral density from computed tomography: application of deep learning with a convolutional neural network, Eur. Radiol. 30 (2020) 3549–3557.
[12] Q. Yao, et al., Radiomics nomogram based on dual-energy spectral CT imaging to diagnose low bone mineral density, BMC Muscoskel. Disord. 23 (2022) 424.
[13] M.M. Lell, G. Jost, J.G. Korporaal, et al., Optimizing contrast media injectionprotocols in state-of-the art CTA, Invest. Radiol. 50 (3) (2015) 161–167.
[14] B. Bodelle, J.L. Wichmann, N. Klotz, et al., Seventykilovolt ultra-low dose CT of the paranasal sinus: first clinical results, Clin. Radiol. 70 (7) (2015) 711–715.
[15] X.G. Cheng, H. Yuan, J. Cheng, et al., Chinese expert consensus on the diagnosis of osteoporosis by imaging and bone mineral density, Quant. Imag. Med. Surg. 10 (10) (2020) 2066–2077.
[16] R. Debnath, N. Takahide, H. Takahashi, A decision based one-against-one method for multi-class support vector machine, CA 7 (2004) 164–175.
[17] Y. Liu, Y.F. Zheng, One-against-all multi-class SVM classification using reliability measures, in: IEEE International Joint Conference on Neural Networks, 2005.
[18] K. Engelke, J.E. Adams, G. Armbrecht, et al., Clinical use of quantitative computed tomography and peripheral quantitative computed tomography in the management of osteoporosis in adults: the 2007 ISCD Official Positions, J. Clin. Densitometry 11 (2008) 123–162.
[19] X. Li, et al., The accuracy of bone mineral density measurement using dual-energy spectral CT and quantitative CT: a comparative phantom study, Clin. Radiol. 75 (2020), 320.e9-320.e15.
[20] Z.H. Zhang, Z.H. Liu, N. Li, et al., Expert consensus on the diagnosis of osteoporosis in Chinese population (3rd edition), Chin. J. Osteoporos. 20 (9) (2014) 1007–1010.
[21] D. Zopfs, S. Lennartz, C. Zaeske, M. Merkt, K.R. Laukamp, R.P. Reimer, D. Maintz, J. Borggrefe, N. Grosse Hokamp, Phantomless assessment of volumetric bone mineral density using virtual non-contrast images from spectral detector computed tomography, Br. J. Radiol. 93 (1109) (2020), 20190992, https://doi.org/10.1259/bjr.20190992. Epub 2020 Mar 4. PMID: 32101453; PMCID: PMC7217579.
[22] X.G. Cheng, et al., Application of low dose chest CT combined with quantitative CT in health management, Chin. J. Health Manag. 16 (9) (2002) 593–595.